

Supplementary Material

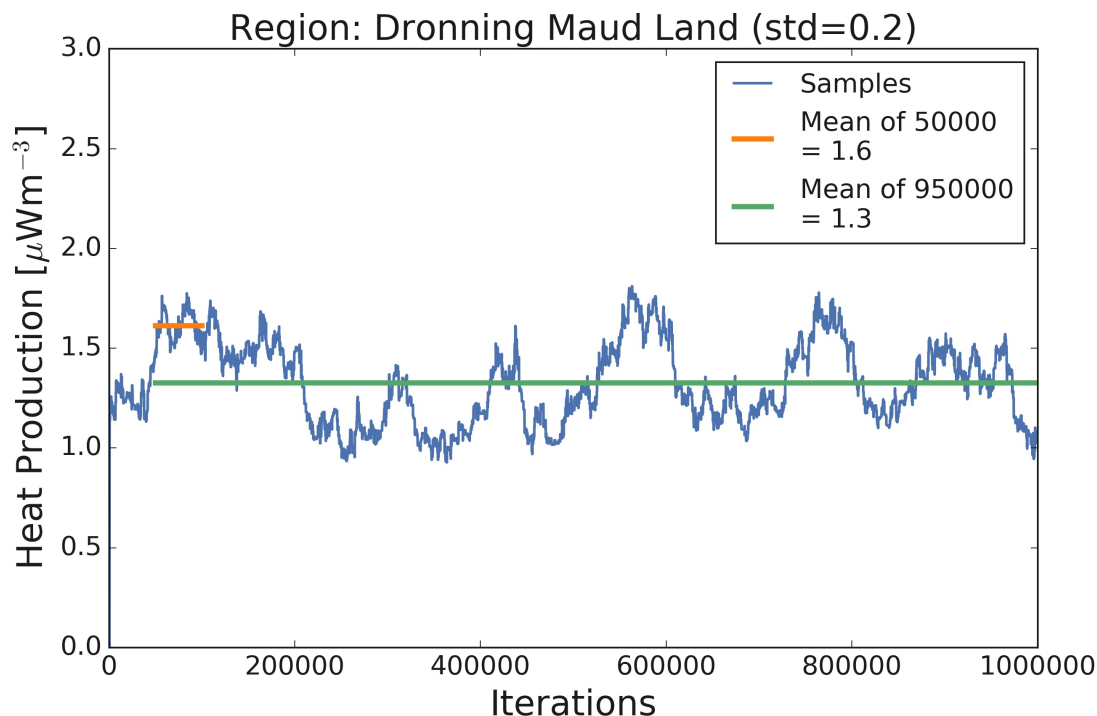


Figure S1. Inversion with 1,000,000 iterations for one column representative for the Dronning Maud Land region (Curie = 30 km, Moho = 40 km, LAB = 180 km) over the heat production parameter (blue line). The first 50,000 iterations are discarded and the mean over the remaining 50,000 (if we would only use 100,000 iterations) and 950,000 is taken as resulting parameters for this location (orange and green lines, respectively). The number of total iterations influences the resulting mean value in this case notably. For the smaller number of iterations it ended up in a local maximum and lies about $0.3 \mu\text{Wm}^{-3}$ (slightly higher than the standard deviation) above the other value.

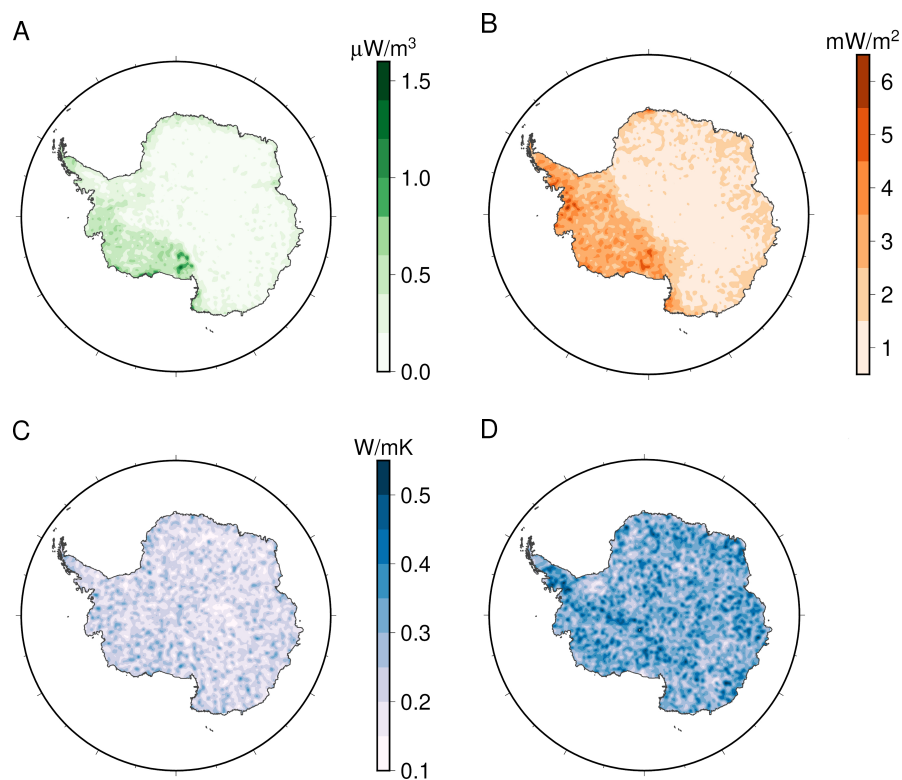


Figure S2. Standard deviations of the output thermal parameters from the inversion for the AN1 model. (A) surface heat production, (B) mantle heat flux, (C) crustal thermal conductivity and (D) mantle thermal conductivity.

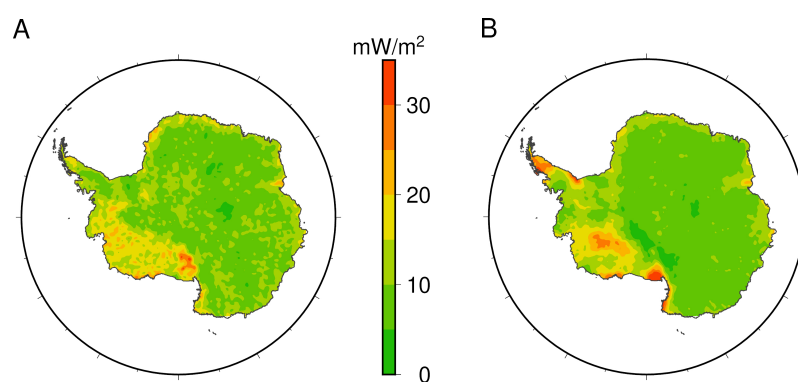


Figure S3. Uncertainty of the calculated surface heat flux from the inversion of (A) the AN1 model and (B) the AN1 model with the Martos Curie depth. For this, standard deviations of the thermal parameters are used, as well as a Moho uncertainty of 5 km.

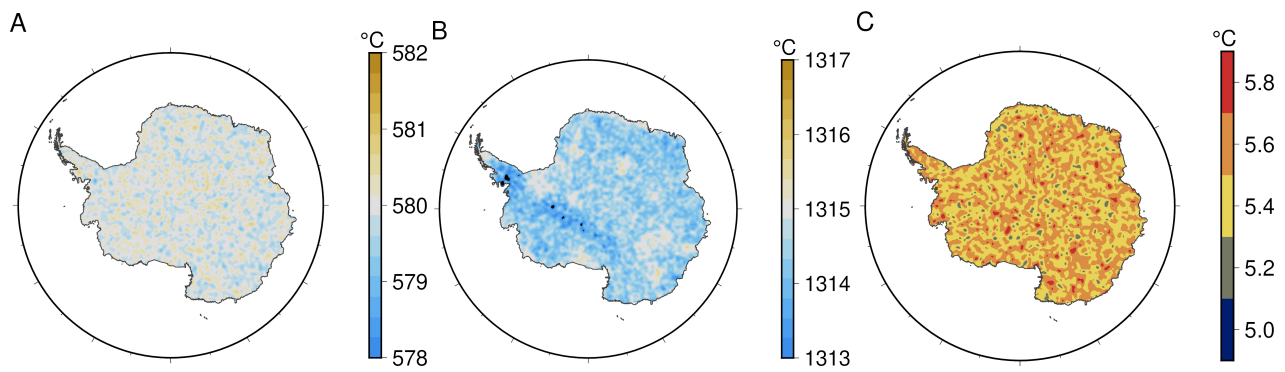


Figure S4. Fitted temperature distributions for the AN1 model at (A) the Curie isotherm and (B) the LAB after 1,000,000 iterations with goal temperatures of 580°C and 1315°C. (C) The mean allowed standard deviation of the temperature fit σ_T .

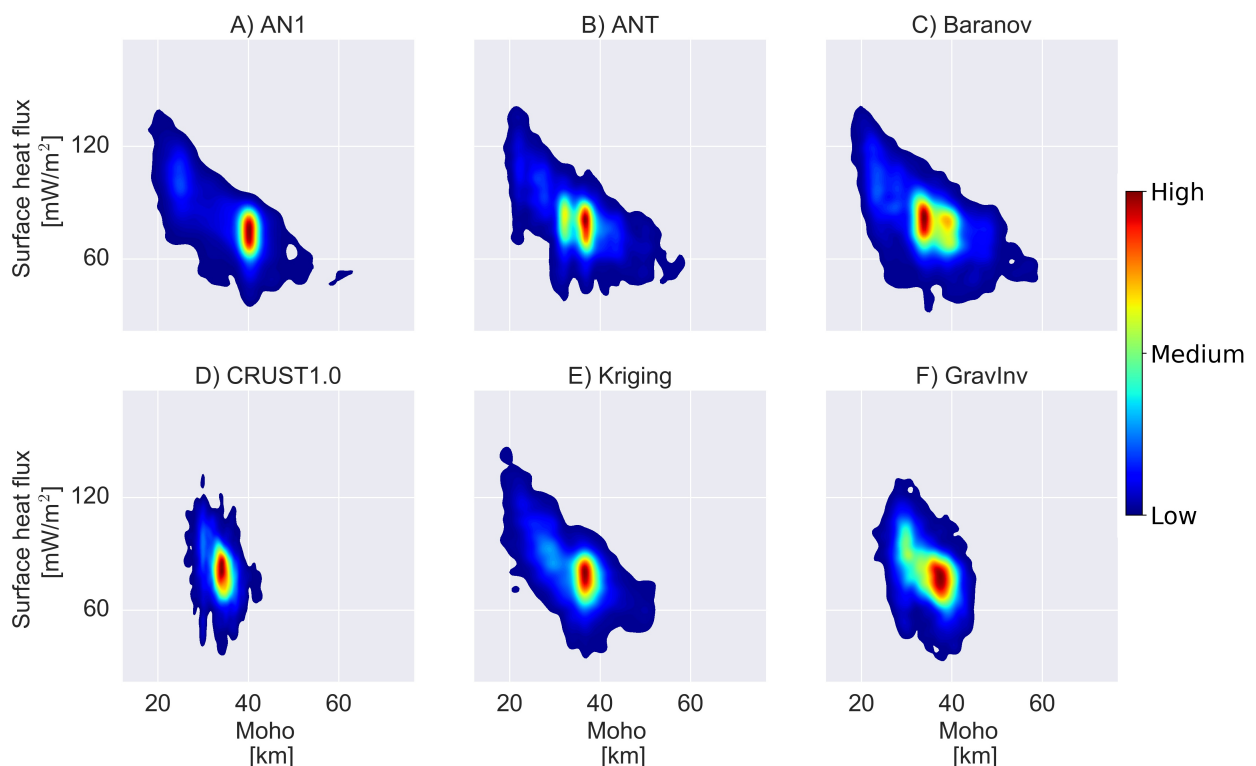


Figure S5. Density plot of the relation between Moho depth and surface heat flux for the inversion results of the AN1 model showing their anticorrelation for different Moho depths. Different models influence the shape of the correlation but not the resulting surface heat flux magnitudes and spatial distribution.

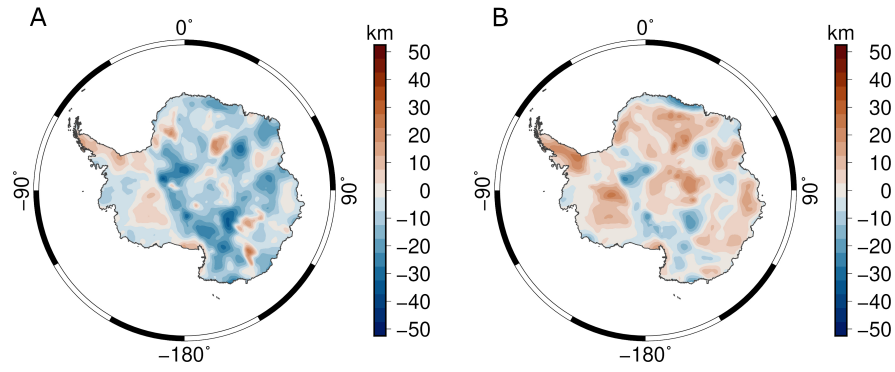


Figure S6. Difference between (A) the Curie depths from the seismological model AN1 and the magnetic Martos model (AN1 - Martos), (B) between the AN1 Moho and the Martos Curie depth (AN1 - Martos).

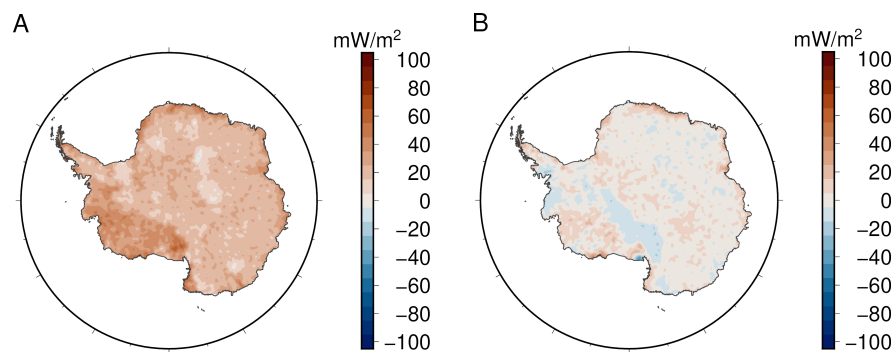


Figure S7. Difference between (A) the seismologically derived geothermal surface heat flux from the study of An et al. (2015) and the modelled heat flux (modelled AN1 - An et al. (2015)) and (B) the magnetically derived geothermal surface heat flux from the study of Martos et al. (2017) and the modelled heat flux (modelled AN1 with Martos Curie - results from Martos et al. (2017)).

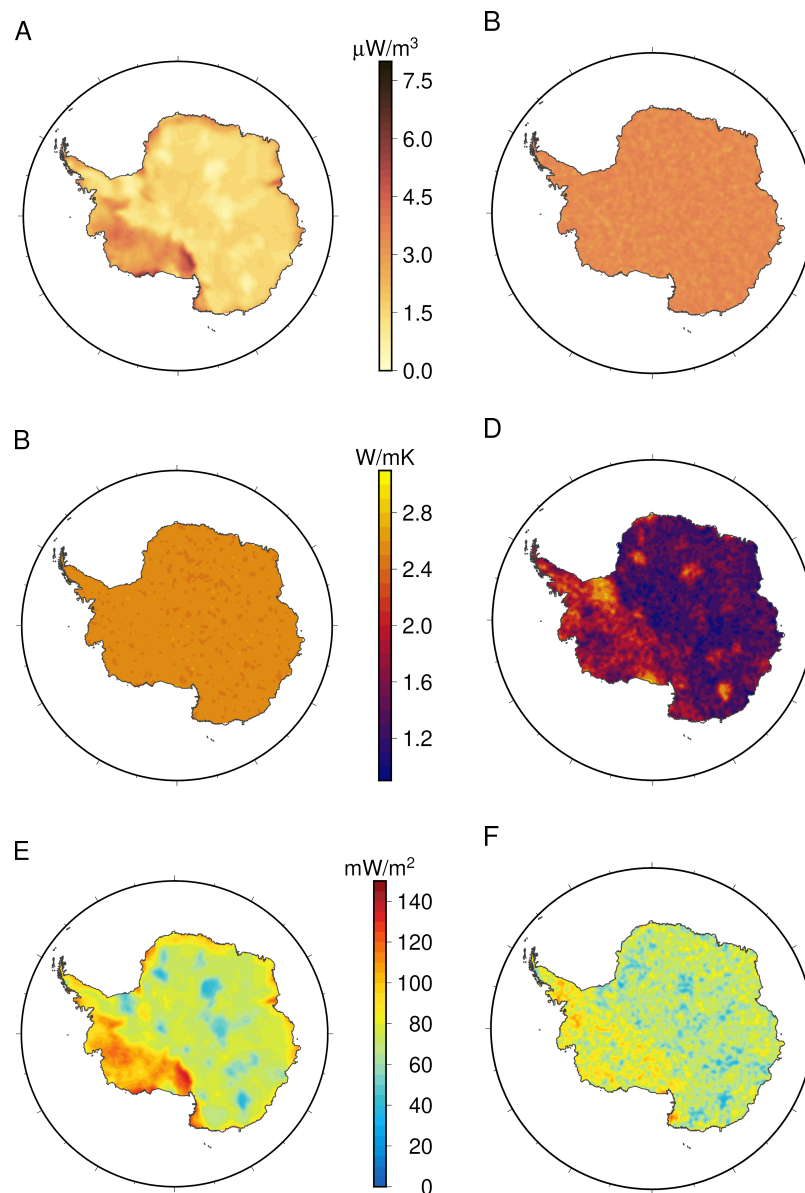


Figure S8. Thermal parameters from the inversion with the AN1 model. Left: with constant heat production within one column. Right: with exponentially decreasing heat production values. (A)+(B) Heat production for the whole crust (top left), only at the surface (top right), (C)+(D) crustal thermal conductivity and (E)+(F) surface heat flux.

REFERENCES

- An, D. A., M. an Wiens, Zhao, Y., Feng, M., Nyblade, A., Kanao, M., Li, Y., et al. (2015). Temperature, lithosphere-asthenosphere boundary, and heat flux beneath the antarctic plate inferred from seismic velocities. *Journal of Geophysical Research: Solid Earth* 120, 8720–8742. doi:10.1002/2015JB011917
- Martos, Y. M., Catalán, M., Jordan, T. A., Golynsky, A., Golynsky, D., Eagles, G., et al. (2017). Heat flux distribution of antarctica unveiled. *Geophysical Research Letters* 44. doi:10.1002/2017GL075609